Predicting the structure of fluids with piecewise constant interactions: Comparing the accuracy of five efficient integral equation theories

Kyle B. Hollingshead and Thomas M. Truskett

Predicting the structure of fluids with piecewise constant interactions: Comparing the accuracy of five efficient integral equation theories

Kyle B. Hollingshead and Thomas M. Truskett*

McKetta Department of Chemical Engineering, University of Texas at Austin, Austin, Texas 78712, USA

We use molecular dynamics simulations to test integral equation theory predictions for the structure of fluids of spherical particles with eight different piecewise-constant pair interaction forms comprising a hard core and a combination of two shoulders and/or wells. Since model pair potentials like these are of interest for discretized or coarse-grained representations of effective interactions in complex fluids (e.g., for computationally intensive inverse optimization problems), we focus here on assessing how accurately their properties can be predicted by analytical or simple numerical closures including Percus-Yevick, hypernetted chain, reference hypernetted chain, first-order mean spherical approximation, and a modified first-order mean spherical approximation. To make quantitative comparisons between the predicted and simulated radial distribution functions, we introduce a cumulative structural error metric. For equilibrium fluid state points of these models, we find that the reference hypernetted chain closure is the most accurate of the tested approximations as characterized by this metric or related thermodynamic quantities.

I. INTRODUCTION

A common challenge in materials science is the "inverse design problem" [1, 2], wherein one seeks to use theoretical models to discover the microscopic characteristics (e.g., the effective pair interactions) of a new system which, if fabricated or synthesized, would yield a targeted material property. Recent applications include designing materials that self-assemble into specific crystalline lattices [3–6], fluids that display optimized structural correlations and related transport properties [7–9], or solids that exhibit specific optical characteristics [10]. Inverse design problems are commonly addressed by stochastic optimization strategies like simulated annealing. Such approaches have the advantage of being general and easy to apply, and they can also be effective as long as material properties required for evaluating the objective function can be accurately and efficiently computed for large numbers of trial interactions during the optimization. This requirement typically means that "exact" yet computationally intensive methods for property determination (e.g., molecular simulations) are impractical for use within such calculations. Approximate theories with analytical or simple numerical solutions are attractive alternatives to molecular simulation in these contexts, provided that they can make sufficiently accurate predictions for a wide range of microscopic interaction types.

For bulk fluids, a key aim for property prediction is to discover the one-to-one link [11] between $g(r)$, the radial distribution function (RDF) of a system at a given set of conditions, and $\varphi(r)$, the interparticle pair potential. Knowledge of these functions of interparticle separation r allows for the direct calculation of the static structure factor, the energy, the pressure, and the isothermal compressibility [12]. Estimations of other properties can be directly obtained from knowledge of the RDF as well.

One example is the two-body excess entropy, which is often a good approximation of the total excess entropy [13] for simple liquids. Another is the information-theoretic estimate for the probability $p_n(\Omega)$ of observing n particle centers in a molecular-scale subvolume Ω, a quantity which characterizes the fluid's density fluctuations [14]. Excess entropy, its two-body approximation, and p_0 have been shown to correlate with various dynamic properties of equilibrium fluids, e.g. diffusivity or viscosity [8, 15–31]. Mode-coupling theory also predicts that dynamic phenomena can be directly estimated from knowledge of the static structure factor [32].

With these considerations in mind, herein we use molecular simulations to test the accuracy of RDF predictions for five approximate integral-equation theory closures: Percus-Yevick, hypernetted chain and reference hypernetted chain [12], first-order mean spherical approximation (FMSA) [33], and a modified exponential version of FMSA [34]. Other more resource-intensive theories, like the Rogers-Young and hybrid mean-spherical approximations [35, 36], self-consistent Ornstein-Zernike approaches [12], and thermodynamic perturbation theories [37–39] are not considered here. We apply the simpler five theories listed above to a diverse suite of eight pair potentials previously introduced by Santos et al [40], each composed of a hard core at $r = \sigma$ plus two piecewise constant sections at larger r (i.e. wells or shoulders), that qualitatively mimic some of the features observed in the effective interactions of complex fluid systems. For each interaction, we investigate four thermodynamic state points with various combinations of low and high density and low and high temperature, and we compare the theoretical predictions for the RDF, the energy, and the two-body excess entropy to data from event-driven molecular dynamics simulations. To facilitate the RDF comparisons we introduce a "cumulative squared error" metric, which provides a quantitative characterization of the overall quality of each theoretical prediction. We also assess the accuracy of predictions for the potential energy

* truskett@che.utexas.edu

and the two-body excess entropy.

II. METHODS

A. Integral Equation Theory

Integral equation theories for uniform, isotropic fluids typically involve solving a system of two equations: the Ornstein-Zernike relation,

$$h(r) = c(r) + \rho \int c\left(|\mathbf{r}' - \mathbf{r}|\right) h(r') d\mathbf{r}', \qquad (1)$$

which defines the direct correlation function $c(r)$ in terms of the number density ρ and the total correlation function $h(r) = g(r) - 1$, and a closure, e.g.,

$$h(r) + 1 = \exp\left[-\beta\varphi(r) + h(r) - c(r) + B(r)\right], \qquad (2)$$

which introduces the link to the pair potential $\varphi(r)$, where $\beta = (k_{\mathrm{B}}T)^{-1}$, T is temperature, k_{B} is Boltzmann's constant, and $B(r)$ is the so-called bridge function.

Two common approximations for $B(r)$ are the Percus-Yevick (PY) closure,

$$B_{\mathrm{PY}}(r) = \ln\left[h(r) - c(r) + 1\right] - h(r) + c(r), \qquad (3)$$

and the hypernetted chain (HNC) closure,

$$B_{\mathrm{HNC}}(r) = 0. \qquad (4)$$

Another is the so-called reference hypernetted chain approximation (RHNC), which assumes that the bridge function can be accurately approximated by that of a reference fluid, typically one of hard spheres at the same density:

$$B_{\mathrm{RHNC}}(r) = B_{\mathrm{HS}}(r). \qquad (5)$$

The hard-sphere fluid's bridge function $B_{\mathrm{HS}}(r)$ has been calculated through careful molecular simulations, and multiple parameterizations for its density dependence exist [41–43]. For this work, we employ the analytical parameterization proposed by Malijevský and Labík [41] for the RHNC closure.

With $B(r)$ specified by these closures, we solve the coupled equations (1) and (2) using a rapidly-converging combination of Newton-Raphson and Picard root-finding methods developed by Labík et al. [44].

An alternative strategy is to replace the closure of Eq. 2 with separate expressions. For example, the mean spherical approximation (MSA) assumes the following relations hold,

$$\begin{aligned} g_{\mathrm{MSA}}(r) &= 0 & r < \sigma, \\ c_{\mathrm{MSA}}(r) &= 0 & r \geq \sigma. \end{aligned} \qquad (6)$$

By further assuming first-order expansions in the characteristic dimensionless energy of the potential $\beta\varepsilon$ for both $g(r)$ and $c(r)$–e.g., $g_{\mathrm{FMSA}}(r) = g_{\mathrm{HS}}(r) + \beta\varepsilon g_1(r)$, where $g_{\mathrm{HS}}(r)$ is the pair correlation function for a hard sphere system at the same density–Tang and Lu closed the equations analytically for several common pair interactions, including square wells [33]. We refer to this solution as the first-order mean spherical approximation (FMSA). In principle, FMSA can be applied to potentials with square shoulders as well. But for strong interactions, FMSA is known to incorrectly predict RDFs with negative values for some interparticle separations [34]. To resolve this, Hlushak et al. modified the FMSA to make it equally applicable to wells and shoulders by rearranging the terms in the series expansion, so that $g_{\mathrm{EFMSA}}(r) = g_{\mathrm{HS}}(r)\exp[-\beta\varepsilon g_1(r)]$ [34]. In this work, we refer to this analytical solution as the exponential first-order mean spherical approximation (EFMSA).

B. Suite of Two-Step Potentials

Motivated by Santos et al. [40], we examine predictions for fluids from a set of pair interactions comprising a hard core and two piecewise-constant steps,

$$\varphi(r) = \begin{cases} \infty & r < \sigma, \\ \varepsilon_1 & \sigma \leq r < \lambda_1, \\ \varepsilon_2 & \lambda_1 \leq r < \lambda_2, \\ 0 & r \geq \lambda_2, \end{cases} \qquad (7)$$

where ε_1 and ε_2 are the energies of the first and second steps, respectively, and λ_1 and λ_2 are the outer edges of the first and second steps, respectively.

Furthermore, as in Santos et al., we restrict the values of ε_i to the set $\{-\varepsilon, -\varepsilon/2, 0, \varepsilon/2, \varepsilon\}$, where ε is a characteristic energy scale. Cases where $\varepsilon_1 = \varepsilon_2$ or $\varepsilon_2 = 0$ reduce to either single square wells or shoulders, or hard spheres, which have all been studied extensively elsewhere (see, e.g., refs. 1-41 in [45]) and are not considered here. We also exclude cases where $\max\{|\varepsilon_1|, |\varepsilon_2|\} = \varepsilon/2$. Of the cases where ε_1 and ε_2 have opposite sign, we consider only combinations where $\varepsilon_2 = -\varepsilon_1 = \pm\varepsilon$. We choose $\lambda_1 = 1.5\sigma$ and $\lambda_2 = 2\sigma$ in order to provide challenging perturbations to the bare hard sphere system that are still amenable to molecular simulation and theoretical treatment. After imposing these restrictions, the remaining eight pairwise interactions shown in Fig. 1, which we refer to as "Type A–H," form our test suite.

To explore how the accuracy of the various theories varies with density and temperature, we investigate each interaction at the four state points comprising combinations of packing fraction $\eta = \rho\pi\sigma^3/6 = 0.15$ or 0.45 and dimensionless temperature $T^* = k_{\mathrm{B}}T/\varepsilon = 0.67$ or 2.0.

C. Molecular Simulations

We compare the theoretical predictions for the RDF, the energy, and the two-body excess entropy to the results of event-driven molecular dynamics simulations per-
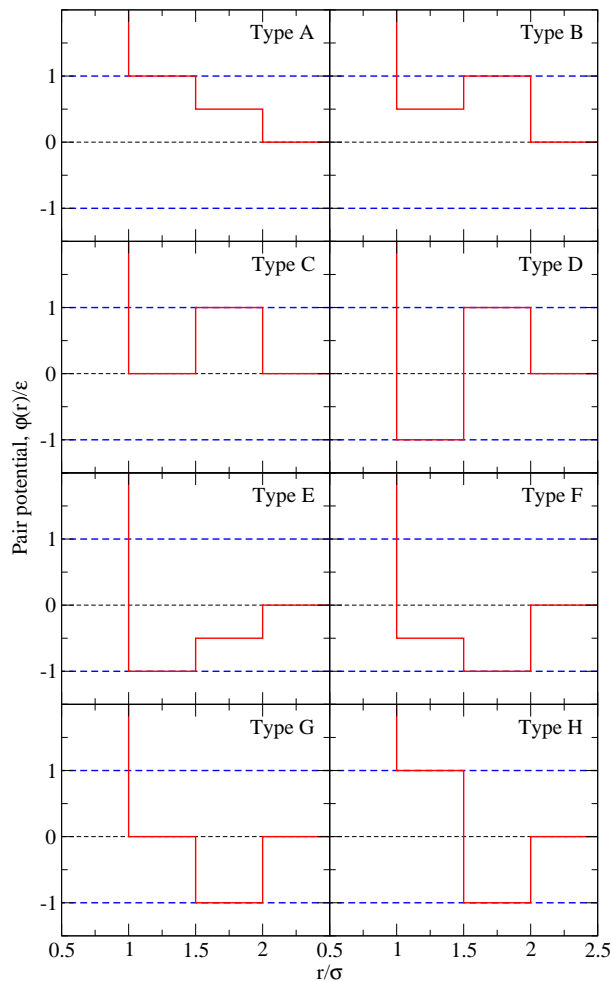
FIG. 1. The suite of eight pair interactions considered in this study, inspired by Santos et al. [40], is topologically exhaustive (e.g., there are no other qualitative arrangements of two constant pairwise pieces that are not more appropriately labeled single wells or shoulders). For each of the eight interactions, the dimensionless pair potential is shown by the red (solid) line.

formed with the DynamO simulation engine [46]. Periodic boundary conditions were used, and the simulated systems were sized such that adequate RDF statistics could be collected for separations up to at least $r = 10\sigma$. In practice, this required $N = 4000$ particles when $\eta = 0.15$, and $N = 8788$ particles when $\eta = 0.45$. The "bins" for particle counts were 0.005σ wide. Temperatures were set and maintained using an Andersen thermostat [47].

Each simulation was initialized as an FCC lattice of the desired density at a high temperature, with randomly assigned particle velocities. After equilibrating for ten million events, the simulations were cooled to the desired temperature and re-equilibrated for a further ten million events. Then, the thermostat was removed, and the RDF was measured over the final five million events. Only isotropic, single-phase fluids were considered in the

comparisons with theory. Those state points determined to be in two-phase (or non-fluid) regions of the phase diagram via analysis of the spatial distribution of particle density or the static structure factor were not considered.

D. Quantifying Error in Predictions

To compare the various RDF theoretical predictions to simulations at a given state point, we define a metric we call the cumulative squared error, $\mathrm{CSE}(r)$:

$$\mathrm{CSE}(r) = \frac{\int_\sigma^r [h_{\mathrm{sim}}(r') - h_{\mathrm{thy}}(r')]^2 r'^2 \, dr'}{\int_\sigma^\infty h_{\mathrm{sim}}^2(r') r'^2 \, dr'}. \quad (8)$$

The integrand in the numerator characterizes the squared deviation in the total correlation function between the prediction of a given theory $h_{\mathrm{thy}}(r)$ and the result of the 'exact' simulation $h_{\mathrm{sim}}(r)$; the power of two eliminates any possible cancellation of error, e.g. for cases where a theory both underpredicts and overpredicts the value of $h(r)$ at different values of r. The denominator accumulates the total squared correlations in the simulated system, and thus normalizes the overall function to facilitate comparison between systems with different degrees of correlation (e.g., between low-density and high-density systems).

As r approaches infinity, all $h(r)$ curves converge to zero and the CSE converges to a finite value, CSE_∞:

$$\mathrm{CSE}_\infty = \lim_{r\to\infty} \mathrm{CSE}(r), \quad (9)$$

which is a measure of the summed squared correlations as a fraction of the total squared correlations in the system; thus, a larger value of CSE_∞ indicates that a theoretical prediction deviates more significantly from the "exact" simulation results. By construction, CSE_∞ has a defined minimum of 0 and, while it does not have a rigorous maximum, its value is typically less than 1 except in cases where the theoretical predictions are qualitatively very poor.

We also calculate the static structure factor $S(k)$ [from which one can obtain the isothermal compressibility $\chi_T = S(0)/(\rho k_B T)$], the potential energy per particle U/ε, the two-body contribution to excess entropy $s^{(2)}/k_B$, and the compressibility factor, $Z = \beta P/\rho$, from simulations and theoretical predictions. The potential energy per particle is

$$\frac{U}{\varepsilon} = \frac{\rho}{2} \int_0^\infty \frac{\varphi(r)}{\varepsilon} g(r) \, d\mathbf{r}, \quad (10)$$

the two-body contribution to excess energy is

$$\frac{s^{(2)}}{k_B} = -\frac{\rho}{2} \int_0^\infty [g(r) \ln g(r) - g(r) + 1] \, d\mathbf{r}, \quad (11)$$

and the compressibility factor is

$$Z = 1 + \frac{2\pi\rho}{3}\sum_{i=0}^{2}\lambda_i{}^3\left[g(\lambda_i^+) - g(\lambda_i^-)\right], \qquad (12)$$

where the superscripts $^-$ or $^+$ indicate the limiting values taken from the left or right of each discontinuity, respectively, and $\lambda_0 = \sigma$. All three quantities can also be directly computed from $g(r)$ and thus, the normalized absolute deviation of the predicted versus simulated values can be used as an indication of the success of theoretical predictions. However, note that different RDFs can, in principle, give rise to the same value of U/ε, $s^{(2)}/k_{\mathrm{B}}$, or Z. Moreover, U/ε only depends on correlations within the range of the pair interaction, and Z only depends on the magnitudes of the discontinuities in the correlations. As a result, we argue here that since the RDF is weighted differently for each thermodynamic quantity, the CSE metric we introduce–which tests the overall similarity between predicted and simulated RDFs–represents a more sensitive measure for the overall predictive quality of particular theory.

III. RESULTS AND DISCUSSION

Structural predictions for the Type A pair interaction are compared to simulation results in Fig. 2 and 3, along with the corresponding cumulative squared errors as calculated via Eq. (8). For this interaction, the analytic solutions (FMSA and EFMSA) perform better at higher rather than at lower equilibrium fluid densities. As density increases, the effect of the excluded volume captured by the well-modeled hard-sphere RDF, $g_{\mathrm{HS}}(r)$, overwhelm the energetic perturbations from the repulsive steps and dominate the resulting structure. Of the tested integral-equation theories with simple numerical closures, the PY closure tends to perform least well near contact, and for interaction Type A, the RHNC offers the best predictions at all four state points investigated. Analogous figures for each of the other interactions are presented for the interested reader in Appendix A.

It is tempting to conclude from a visual comparison of theoretical and simulated radial distribution functions that all of the theories perform similarly well, especially at the higher temperature (Figs. 2d and 2h). However, the resulting CSEs differ *by nearly two orders of magnitude* from most to least accurate (Figs. 2c and 2g), which underscores the utility and sensitivity of the CSE metric. As discussed below, these differences in the CSE become important when computing other quantities that depend on the RDF, especially when one considers that each thermodynamic quantity weights the RDF in a different way.

The total cumulative squared errors CSE_∞ for all interactions, state points, and theories are listed in Table I. Six of the total thirty-two combinations of interaction
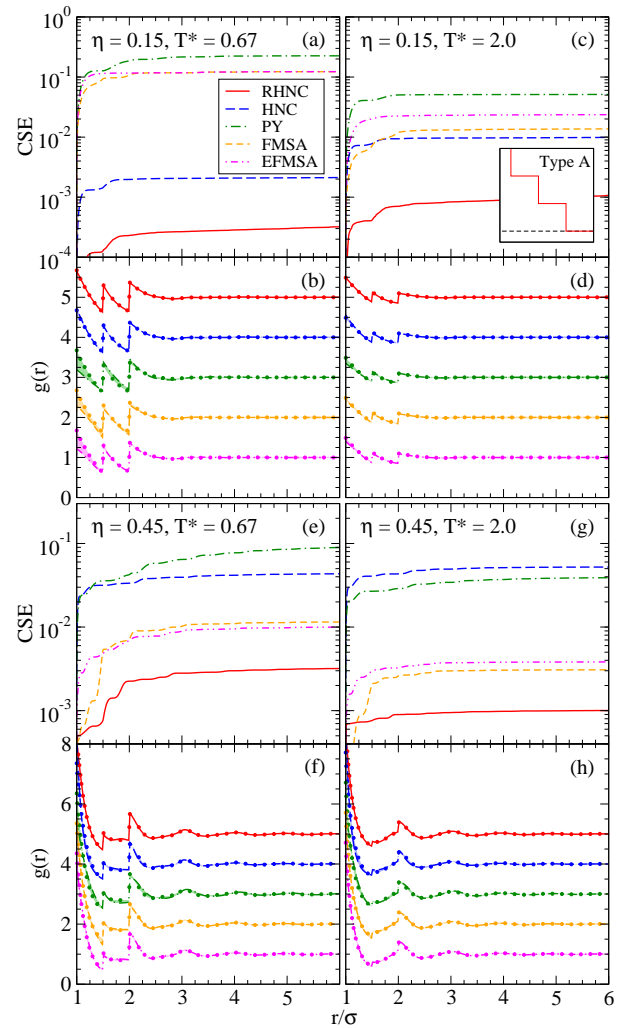

FIG. 2. Radial distribution functions $g(r) = h(r) + 1$ and the associated cumulative squared errors (CSE, see Eq. (8)) predicted by the reference hypernetted chain (RHNC), hypernetted chain (HNC), and Percus-Yevick (PY) Ornstein-Zernike closures [12, 41]; the first-order mean spherical approximation solution (FMSA) [33]; and the simple exponential first-order mean spherical approximation (EFMSA) [34], for the "type A" pair interaction. For clarity, unit vertical offsets were applied to the RDF curves, and they are stacked in the same order (top-to-bottom) as listed in the legend. The simulated RDF (solid circles) for this state point is reproduced five times to compare with each vertically offset theoretical RDF; shaded regions adjacent to each $g(r)$ highlight the differences between each theory and simulation results.

type and state point considered did not produce single-phase, uniform fluids when simulated. Of the remaining twenty-six systems, the RHNC offered the most accurate structural predictions for all but four; however, at three of these four points, the CSE_∞ of the RHNC is still within ca. 65% of the most accurate theory (HNC). All four points are at low temperature ($T^* = 0.67$) and high packing fraction ($\eta = 0.45$), and each of the pair
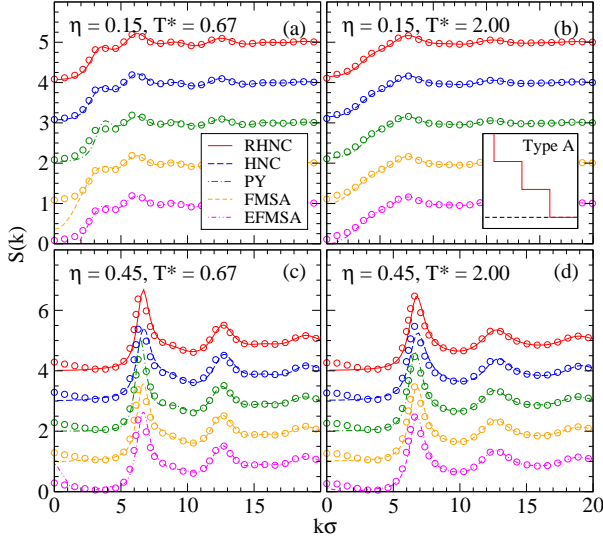
FIG. 3. Structure factors $S(k)$ predicted by the reference hypernetted chain (RHNC), hypernetted chain (HNC), and Percus-Yevick (PY) Ornstein-Zernike closures [12, 41]; the first-order mean spherical approximation solution (FMSA) [33]; and the simple exponential first-order mean spherical approximation (EFMSA) [34], for the "type A" pair interaction. For clarity, unit vertical offsets were applied to the structure factor curves, and they are stacked in the same order (top-to-bottom) as listed in the legend. The simulated structure factor (open circles) for this state point is reproduced five times to compare with each vertically offset theoretical $S(k)$.

interactions include attractions (types D, F, G, and H).

We also compare CSE_∞ against the absolute normalized errors for predictions of three example thermodynamic quantities: two-body excess entropy $s^{(2)}/k_B$, potential energy U/ε, and compressibility factor (i.e., normalized pressure) Z, in Fig. 4. Fig. 4a shows that CSE_∞ is generally a good predictor of $s^{(2)}/k_B$ accuracy, although there are a handful of instances where the fractional error in the excess entropy is low while CSE_∞ is higher. The correlations between CSE_∞ and the potential energy or pressure are a bit weaker, but still present; this is likely due to opportunities for fortuitous cancellation of error when pair interactions contain both positive and negative contributions (e.g., types D and H), when portions of the interactions are zero (types C and G), or when significant contributions to CSE_∞ occur beyond the range of the pair interaction. Overall, however, it is clear that the accuracies of both example thermodynamic quantity predictions correlate well with the cumulative squared error. For the interested reader, the values of excess entropy, potential energy, and compressibility factor errors are tabulated in Appendix B.

TABLE I. Total cumulative squared errors (CSE_∞) for all theoretical approaches, thermodynamic state points, and interactions considered. "R," "H," and "P" are the RHNC [12, 41], HNC [12], and PY [12] closures to the Ornstein-Zernike relation, respectively. "F" is the FMSA [33], and "E" is the EFMSA [34]. Italics indicate the lowest value of CSE_∞ (and hence the theory with the most accurate structural prediction) at each combination of state point and interaction type.

	Type A				Type B			
T^*	0.67		2.00		0.67		2.00	
η	0.15	0.45	0.15	0.45	0.15	0.45	0.15	0.45
R	*0.000*	*0.003*	*0.002*	*0.001*	*0.001*	*0.011*	*0.000*	*0.002*
H	0.002	0.044	0.010	0.052	*0.001*	0.039	0.001	0.059
P	0.226	0.093	0.052	0.039	0.013	0.021	0.005	0.007
F	0.123	0.012	0.014	0.003	0.092	0.053	0.010	0.006
E	0.123	0.010	0.024	0.004	0.082	0.097	0.008	0.011

	Type C				Type D			
T^*	0.67		2.00		0.67		2.00	
η	0.15	0.45	0.15	0.45	0.15	0.45	0.15	0.45
R	*0.002*	*0.010*	*0.000*	*0.003*	*0.079*	0.046	*0.001*	*0.004*
H	0.003	0.024	0.001	0.061	0.083	*0.030*	0.002	0.057
P	0.005	0.019	0.001	0.004	0.092	0.197	0.002	0.019
F	0.096	0.081	0.008	0.009	0.168[b]	0.269[b]	0.016	0.018
E	0.184	0.160	0.015	0.016	0.412	0.522	0.040	0.032

	Type E				Type F			
T^*	0.67		2.00		0.67		2.00	
η	0.15	0.45	0.15	0.45	0.15	0.45	0.15	0.45
R	—[a]	—[a]	—[a]	*0.001*	—[a]	0.094	—[a]	*0.004*
H	—[a]	—[a]	—[a]	0.067	—[a]	*0.027*	—[a]	0.048
P	—[a]	—[a]	—[a]	0.020	—[a]	0.268	—[a]	0.049
F	—[a]	—[a]	—[a]	0.004	—[a]	0.287	—[a]	0.027
E	—[a]	—[a]	—[a]	0.002	—[a]	0.113	—[a]	0.011

	Type G				Type H			
T^*	0.67		2.00		0.67		2.00	
η	0.15	0.45	0.15	0.45	0.15	0.45	0.15	0.45
R	—[a]	0.023	*0.001*	*0.007*	*0.053*	0.056	*0.004*	*0.014*
H	—[a]	*0.010*	0.008	0.040	0.063	*0.024*	0.008	0.027
P	—[a]	0.388	0.007	0.090	0.104	0.781	0.009	0.204
F	—[a]	0.256[b]	0.018	0.039	0.208[b]	0.507[b]	0.031	0.078
E	—[a]	0.174	0.020	0.019	0.750	0.405	0.044	0.044

[a] Simulated system is not a single-phase, uniform fluid at equilibrium.
[b] Theory predicts an unphysical RDF, i.e. $g(r) < 0$ for some r.

IV. CONCLUSION

In order to quantify the overall accuracy of theoretical predictions for fluid structure, we have introduced the total cumulative squared error (CSE_∞) metric, which accumulates squared discrepancies between a theoretical prediction and a reference "exact" result at all separation distances along the total correlation function and avoids any possible cancellation of error. We find that this CSE_∞ metric is very sensitive and tends to forecast the overall accuracy of structure-dependent thermodynamic calculations. As a result, it is an excellent tool for
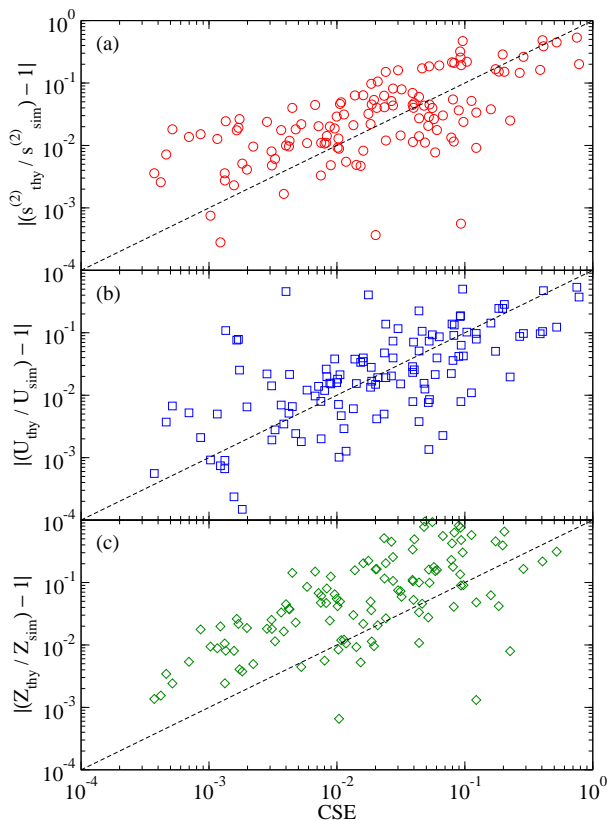
FIG. 4. Correlations between total cumulative squared error CSE_∞ and (a) absolute normalized two-body excess entropy error (circles), (b) absolute normalized potential energy error (squares), and (c) absolute normalized compressibility factor error (diamonds) for all data collected.

comparing accuracy between multiple theories, particularly when differences are difficult to discern by visual inspection.

We have used this metric to test the performance of five integral equation theory-based approaches for predicting equilibrium fluid structure in systems with pair interactions comprising a hard core plus two piecewise constant

interactions, and we find that the reference hypernetted chain (RHNC) integral equation closure offers accurate and efficient predictions across a broad range of interactions and thermodynamic state points. This kind of analysis, i.e., considering the accuracy of various efficient theoretical methods for predicting the structure consistent with a broad range of possible interactions, will be particularly important for inverse design problems where the goal is to rather accurately predict which interaction is consistent with a targeted structure (or structurally-related property).

ACKNOWLEDGMENTS

Appendix A: Extended Type B-H Structure Plots

The predicted radial distribution functions $g(r)$ compared against simulation results, the resulting cumulative squared errors $CSE(r)$, and the corresponding structure factors $S(k)$ are shown for interaction types B through H in Figs. 5–11, respectively.

Appendix B: Complete Thermodynamic Error Tables

In Tables II and III, we present tabulated values for the absolute normalized potential energy and 2-body excess entropy errors, respectively, for all theories and state points considered in this study.

[1] S. Torquato, Soft Matter **5**, 1157 (2009).

[2] A. Jain, J. A. Bollinger, and T. M. Truskett, AIChE Journal **60**, 2732 (2014).

[3] A. Jain, J. R. Errington, and T. M. Truskett, Soft Matter **9** (2013).

[4] E. Marcotte, F. H. Stillinger, and S. Torquato, J. Chem. Phys. **134**, 164105 (2011).

[5] H. Cohn and A. Kumar, Proc. Natl. Acad. Sci. U.S.A. **106**, 9570 (2009).

[6] E. Edlund, O. Lindgren, and M. N. Jacobi, Phys. Rev. Lett. **107**, 085503 (2011).

[7] F. H. Stillinger, S. Torquato, J. M. Eroles, and T. M. Truskett, J. Phys. Chem. B **105**, 6592 (2001).

[8] J. Carmer, G. Goel, M. J. Pond, J. R. Errington, and T. M. Truskett, Soft Matter **8**, 4083 (2012).

[9] G. Goel, W. P. Krekelberg, J. R. Errington, and T. M. Truskett, Phys. Rev. Lett. **100**, 106001 (2008).

[10] J. Andkjær, V. E. Johansen, K. S. Friis, and O. Sigmund, J. Opt. Soc. Am. B **31**, 164 (2014).

[11] R. Henderson, Phys. Lett. A **49**, 197 (1974).

[12] J.-P. Hansen and I. R. McDonald, *Theory of Simple Liquids* (Elsevier Science, 2006).

[13] R. E. Nettleton and M. S. Green, J. Chem. Phys. **29** (1958).

[14] G. Hummer, S. Garde, A. E. Garca, M. E. Paulaitis, and L. R. Pratt, J. Phys. Chem. B **102**, 10469 (1998).

[15] Y. Rosenfeld, Phys. Rev. A **15**, 2545 (1977).
[16] M. Dzugutov, Nature **381**, 137 (1996).
[17] Y. Rosenfeld, J. Phys.: Condens. Matter **11**, 5415 (1999).
[18] R. Sharma, S. N. Chakraborty, and C. Chakravarty, J. Chem. Phys. **125**, 204501 (2006).
[19] E. H. Abramson, Phys. Rev. E **76**, 051203 (2007).
[20] W. P. Krekelberg, J. Mittal, V. Ganesan, and T. M. Truskett, J. Chem. Phys. **127**, 044502 (2007).
[21] E. H. Abramson and H. West-Foyle, Phys. Rev. E **77**, 041202 (2008).
[22] J. Mittal, T. M. Truskett, J. R. Errington, and G. Hummer, Phys. Rev. Lett. **100**, 145901 (2008).
[23] E. H. Abramson, Phys. Rev. E **80**, 021201 (2009).
[24] N. Gnan, T. B. Schrøder, U. R. Pedersen, N. P. Bailey, and J. C. Dyre, J. Chem. Phys. **131**, 234504 (2009).
[25] G. Goel, W. P. Krekelberg, M. J. Pond, J. Mittal, V. K. Shen, J. R. Errington, and T. M. Truskett, J. Stat. Mech. Theor. Exp. **2009**, P04006 (2009).
[26] W. P. Krekelberg, M. J. Pond, G. Goel, V. K. Shen, J. R. Errington, and T. M. Truskett, Phys. Rev. E **80**, 061205 (2009).
[27] M. J. Pond, W. P. Krekelberg, V. K. Shen, J. R. Errington, and T. M. Truskett, J. Chem. Phys. **131**, 161101 (2009).
[28] R. Chopra, T. M. Truskett, and J. R. Errington, J. Chem. Phys. **133**, 104506 (2010).
[29] M. Agarwal, M. Singh, B. S. Jabes, and C. Chakravarty, J. Chem. Phys. **134**, 014502 (2011).
[30] M. J. Pond, J. R. Errington, and T. M. Truskett, J. Chem. Phys. **134**, 081101 (2011).
[31] J. A. Bollinger, A. Jain, and T. M. Truskett, Langmuir **30**, 8247 (2014).
[32] D. R. Reichman and P. Charbonneau, J. Stat. Mech. Theor. Exp. **2005**, P05013 (2005).
[33] Y. Tang and B. C.-Y. Lu, Mol. Phys. **90**, 215 (1997).
[34] S. P. Hlushak, P. A. Hlushak, and A. Trokhymchuk, J. Chem. Phys. **138**, 164107 (2013).
[35] F. J. Rogers and D. A. Young, Phys. Rev. A **30**, 999 (1984).
[36] G. Zerah and J. Hansen, J. Chem. Phys. **84**, 2336 (1986).
[37] W. R. Smith, D. Henderson, and J. A. Barker, J. Chem. Phys. **55** (1971).
[38] S. Zhou, Phys. Rev. E **74**, 031119 (2006).
[39] S. Zhou, Phys. Rev. E **77**, 041110 (2008).
[40] A. Santos, S. B. Yuste, M. L. de Haro, M. Bárcenas, and P. Orea, J. Chem. Phys. **139**, 074505 (2013).
[41] A. Malijevský and S. Labík, Mol. Phys. **60**, 663 (1987).
[42] L. Verlet and J.-J. Weis, Phys. Rev. A **5**, 939 (1972).
[43] D. Henderson and E. W. Grundke, J. Chem. Phys. **63**, 601 (1975).
[44] S. Labík, A. Malijevský, and P. Voňka, Mol. Phys. **56**, 709 (1985).
[45] S. Yuste, A. Santos, and M. López de Haro, Mol. Phys. **109**, 987 (2011).
[46] M. N. Bannerman, R. Sargant, and L. Lue, J. Comput. Chem. **32**, 3329 (2011).
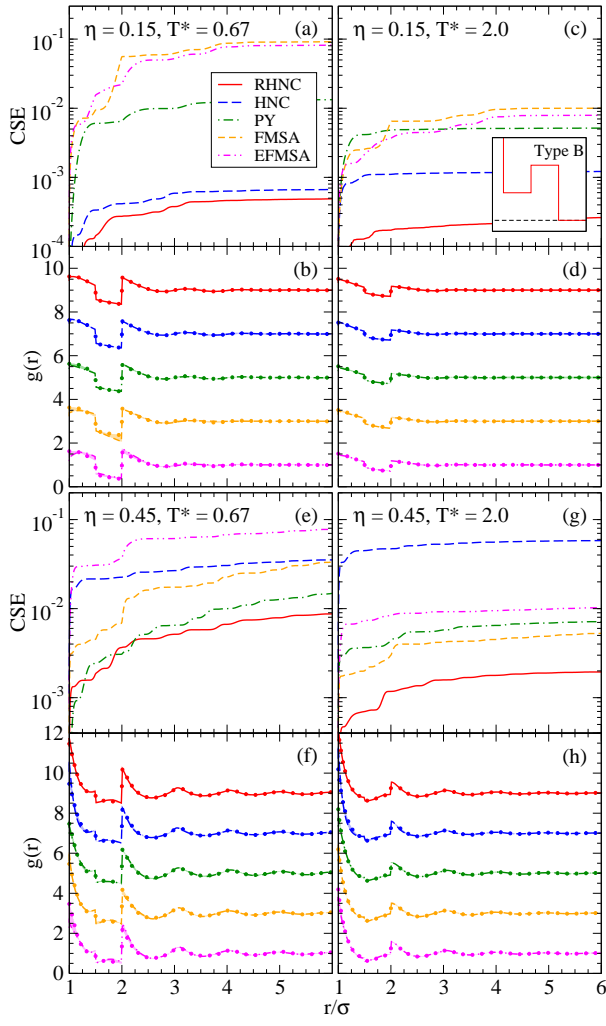[47] H. C. Andersen, J. Chem. Phys. **72**, 2384 (1980).

FIG. 5. Radial distribution functions $g(r) = h(r) + 1$ and the associated cumulative squared errors (CSE, see Eq. (8)) predicted by the reference hypernetted chain (RHNC), hypernetted chain (HNC), and Percus-Yevick (PY) Ornstein-Zernike closures [12, 41]; the first-order mean spherical approximation solution (FMSA) [33]; and the simple exponential first-order mean spherical approximation (EFMSA) [34], for the "type B" pair interaction. For clarity, unit vertical offsets were applied to the RDF curves, and they are stacked in the same order (top-to-bottom) as listed in the legend. The simulated RDF (solid circles) for this state point is reproduced five times to compare with each vertically offset theoretical RDF; shaded regions adjacent to each $g(r)$ highlight the differences between each theory and simulation results.

FIG. 6. Radial distribution functions and cumulative squared errors for the "type C" interaction. Series and labeling are as in Fig. 5.

FIG. 7. Radial distribution functions and cumulative squared errors for the "type D" interaction. Series and labeling are as in Fig. 5.

FIG. 8. Radial distribution functions and cumulative squared errors for the "type E" interaction. Series and labeling are as in Fig. 5.

FIG. 9. Radial distribution functions and cumulative squared errors for the "type F" interaction. Series and labeling are as in Fig. 5.

FIG. 10. Radial distribution functions and cumulative squared errors for the "type G" interaction. Series and labeling are as in Fig. 5.
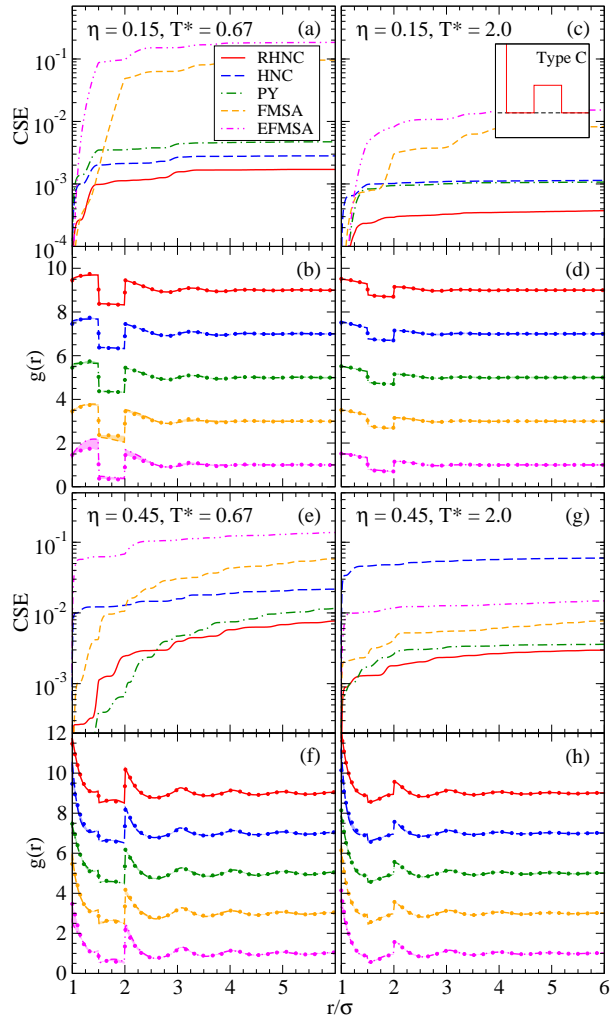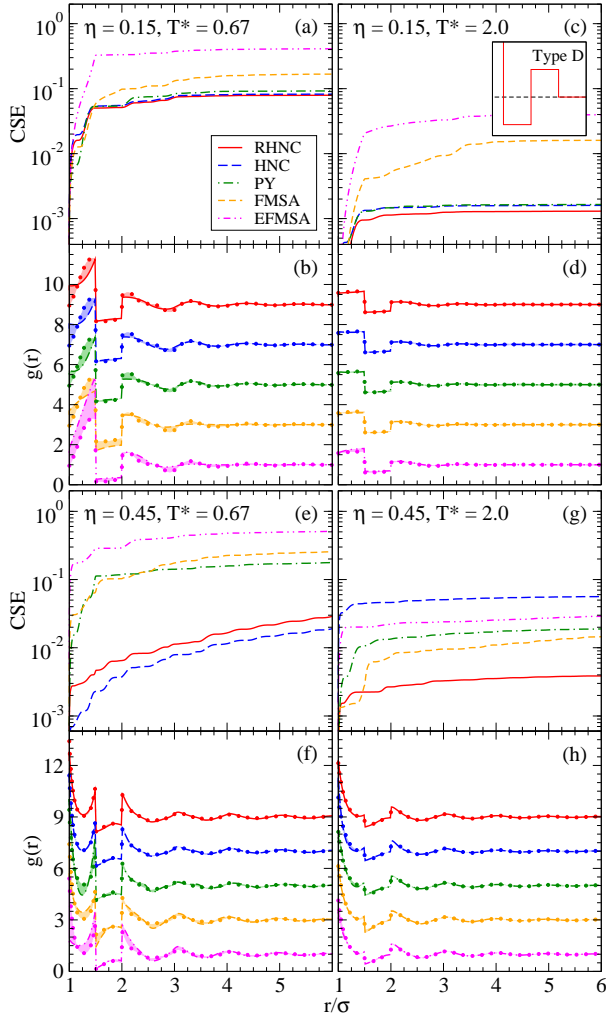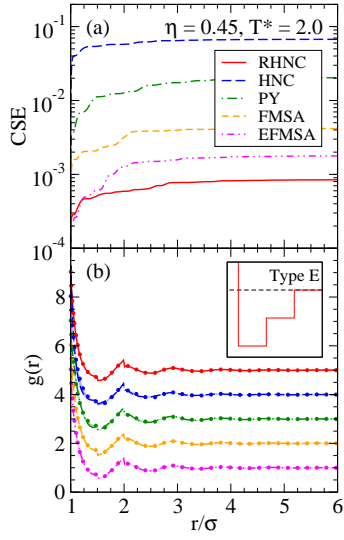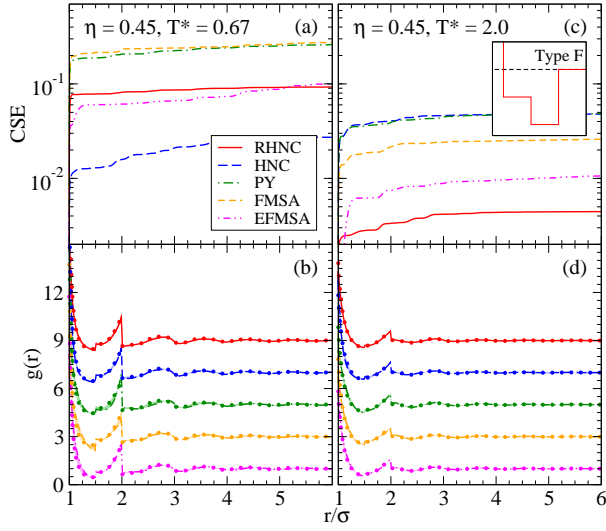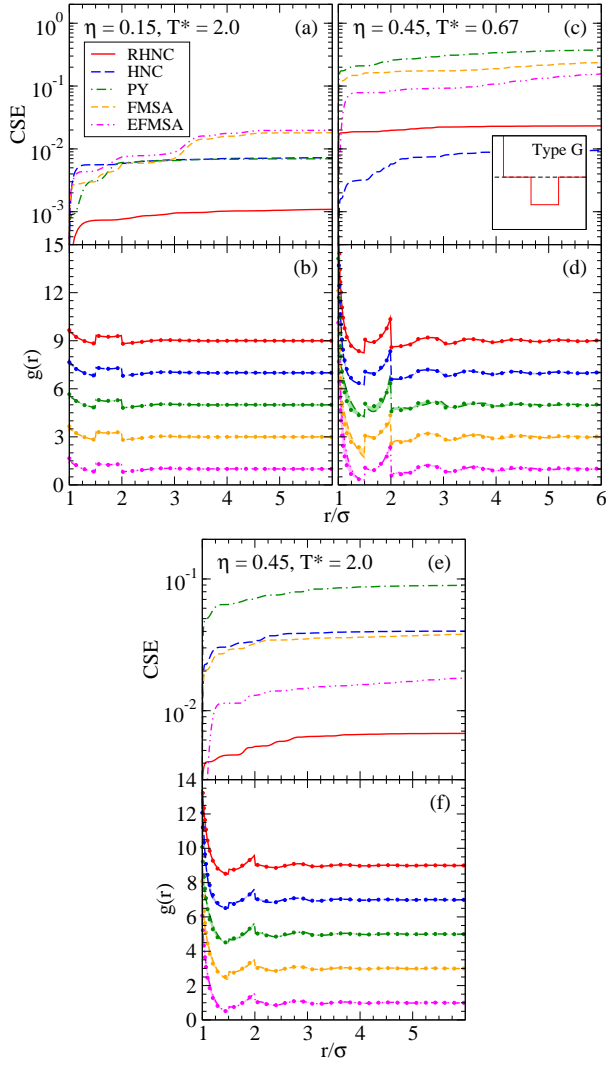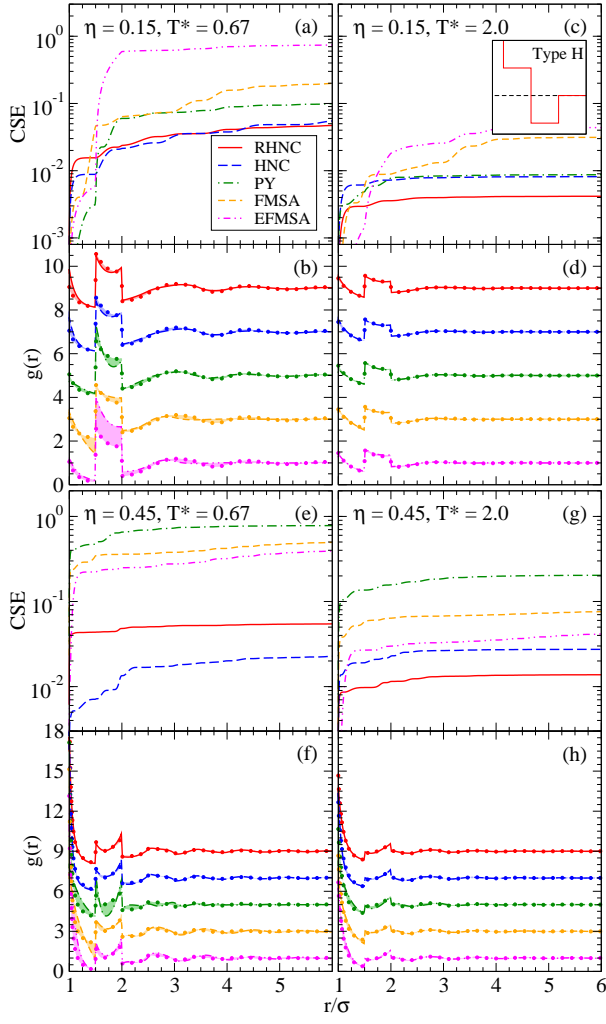
FIG. 11. Radial distribution functions and cumulative squared errors for the "type H" interaction. Series and labeling are as in Fig. 5.

TABLE II. Absolute normalized potential energy error, $|(U_{\text{thy}}/U_{\text{sim}}) - 1|$, for all approaches, state points, and interactions considered. Labels are as in Table I. Italics indicate the value closest to zero (e.g., a perfect prediction) at each combination of state point and interaction type.

	Type A				Type B			
T^*	0.67		2.00		0.67		2.00	
η	0.15	0.45	0.15	0.45	0.15	0.45	0.15	0.45
R	*0.000*	*0.003*	*0.000*	*0.001*	0.007	0.021	*0.001*	0.006
H	*0.000*	0.004	0.001	*0.001*	*0.005*	0.029	*0.001*	0.021
P	0.020	0.008	0.008	0.008	0.006	0.019	0.002	0.008
F	0.098	0.001	0.015	0.002	0.182	*0.009*	0.018	0.012
E	0.079	0.007	0.019	0.003	0.091	0.043	0.012	*0.005*

	Type C				Type D			
T^*	0.67		2.00		0.67		2.00	
η	0.15	0.45	0.15	0.45	0.15	0.45	0.15	0.45
R	0.025	0.038	0.004	0.014	0.138	*0.106*	0.109	0.458
H	0.022	0.048	*0.001*	0.040	*0.133*	0.117	0.076	1.203
P	*0.002*	*0.028*	0.005	*0.007*	0.188	0.246	0.078	1.549
F	0.501	0.036	0.020	0.015	—[b]	—[b]	*0.040*	*0.404*
E	0.245	0.143	0.034	0.035	0.473	0.123	0.071	2.630

	Type E				Type F			
T^*	0.67		2.00		0.67		2.00	
η	0.15	0.45	0.15	0.45	0.15	0.45	0.15	0.45
R	—[a]	—[a]	—[a]	0.002	—[a]	0.063	—[a]	0.007
H	—[a]	—[a]	—[a]	0.002	—[a]	0.040	—[a]	0.016
P	—[a]	—[a]	—[a]	0.004	—[a]	0.087	—[a]	0.013
F	—[a]	—[a]	—[a]	0.005	—[a]	0.097	—[a]	0.020
E	—[a]	—[a]	—[a]	*0.000*	—[a]	*0.011*	—[a]	*0.003*

	Type G				Type H			
T^*	0.67		2.00		0.67		2.00	
η	0.15	0.45	0.15	0.45	0.15	0.45	0.15	0.45
R	—[a]	*0.005*	*0.001*	*0.010*	*0.073*	*0.093*	0.021	0.038
H	—[a]	0.016	0.002	0.025	0.086	0.138	0.026	0.074
P	—[a]	0.096	0.014	0.042	0.102	0.374	0.016	0.284
F	—[a]	—[b]	0.013	0.023	—[b]	—[b]	*0.015*	*0.022*
E	—[a]	0.051	0.015	0.017	0.536	0.105	0.051	0.224

[a] Simulated system is not a single-phase, uniform fluid at equilibrium.
[b] Theory predicts an unphysical RDF, *i.e.* $g(r) < 0$ for some r.

TABLE III. Absolute normalized 2-body excess entropy error, $|(s^{(2)}_{\text{thy}}/s^{(2)}_{\text{sim}}) - 1|$, for all approaches, state points, and interactions considered. Labels are as in Table I. Italics indicate the value closest to zero (e.g., a perfect prediction) at each combination of state point and interaction type.

	Type A				Type B			
T^*	0.67		2.00		0.67		2.00	
η	0.15	0.45	0.15	0.45	0.15	0.45	0.15	0.45
R	*0.003*	0.006	*0.002*	*0.001*	0.018	0.046	*0.004*	0.004
H	0.010	0.014	0.009	0.029	0.014	0.069	*0.004*	0.008
P	0.025	*0.001*	0.021	0.011	0.021	0.106	0.022	*0.003*
F	0.009	0.005	0.005	0.005	0.320	0.045	0.009	0.011
E	0.034	0.013	0.012	0.002	*0.012*	*0.024*	0.011	0.049

	Type C				Type D			
T^*	0.67		2.00		0.67		2.00	
η	0.15	0.45	0.15	0.45	0.15	0.45	0.15	0.45
R	0.026	*0.019*	0.007	0.008	0.215	0.172	0.024	*0.010*
H	0.024	0.041	*0.000*	0.018	*0.210*	*0.160*	0.018	0.027
P	*0.018*	0.097	0.013	0.018	0.255	0.287	0.019	0.054
F	0.470	0.055	0.014	*0.005*	—[b]	—[b]	*0.008*	0.032
E	0.153	0.038	0.005	0.064	0.388	0.448	0.040	0.079

	Type E				Type F			
T^*	0.67		2.00		0.67		2.00	
η	0.15	0.45	0.15	0.45	0.15	0.45	0.15	0.45
R	—[a]	—[a]	—[a]	0.015	—[a]	0.193	—[a]	0.040
H	—[a]	—[a]	—[a]	0.030	—[a]	0.081	—[a]	0.043
P	—[a]	—[a]	—[a]	0.040	—[a]	0.146	—[a]	*0.011*
F	—[a]	—[a]	—[a]	0.010	—[a]	0.263	—[a]	0.051
E	—[a]	—[a]	—[a]	*0.005*	—[a]	*0.052*	—[a]	0.031

	Type G				Type H			
T^*	0.67		2.00		0.67		2.00	
η	0.15	0.45	0.15	0.45	0.15	0.45	0.15	0.45
R	—[a]	0.063	0.003	0.045	*0.185*	*0.040*	0.012	0.063
H	—[a]	*0.029*	0.011	0.048	0.191	0.151	*0.011*	0.044
P	—[a]	0.162	0.020	*0.037*	0.220	0.201	0.020	0.151
F	—[a]	—[b]	0.022	0.045	—[b]	—[b]	0.014	*0.013*
E	—[a]	0.167	*0.000*	0.045	0.533	0.485	0.027	0.060

[a] Simulated system is not a single-phase, uniform fluid at equilibrium.
[b] Theory predicts an unphysical RDF, *i.e.* $g(r) < 0$ for some r.

TABLE IV. Absolute normalized compressibility error, $|(Z_{\mathrm{thy}}/Z_{\mathrm{sim}}) - 1|$, for all approaches, state points, and interactions considered. Labels are as in Table I. Italics indicate the value closest to zero (e.g., a perfect prediction) at each combination of state point and interaction type.

	Type A				Type B			
T^*	0.67		2.00		0.67		2.00	
η	0.15	0.45	0.15	0.45	0.15	0.45	0.15	0.45
R	0.002	0.011	0.008	*0.009*	*0.002*	*0.050*	*0.001*	0.019
H	0.005	0.100	*0.001*	0.161	0.005	0.110	0.011	0.153
P	0.008	0.090	0.028	0.105	0.030	0.021	0.004	0.047
F	*0.001*	0.011	0.009	0.018	0.135	0.099	0.042	0.085
E	0.048	*0.008*	0.027	0.016	0.041	0.091	0.006	*0.012*

	Type C				Type D			
T^*	0.67		2.00		0.67		2.00	
η	0.15	0.45	0.15	0.45	0.15	0.45	0.15	0.45
R	*0.004*	0.065	*0.003*	0.025	*0.424*	*0.046*	*0.008*	0.045
H	0.018	0.116	0.020	0.159	0.630	0.075	0.026	0.177
P	0.023	*0.036*	0.009	0.033	0.756	0.393	0.022	*0.010*
F	0.302	0.178	0.080	0.124	—[b]	—[b]	0.203	0.223
E	0.042	0.063	0.005	*0.022*	4.977	0.312	0.053	0.059

	Type E				Type F			
T^*	0.67		2.00		0.67		2.00	
η	0.15	0.45	0.15	0.45	0.15	0.45	0.15	0.45
R	—[a]	—[a]	—[a]	0.018	—[a]	0.479	—[a]	0.143
H	—[a]	—[a]	—[a]	0.556	—[a]	*0.106*	—[a]	0.777
P	—[a]	—[a]	—[a]	0.164	—[a]	1.680	—[a]	0.950
F	—[a]	—[a]	—[a]	0.038	—[a]	0.165	—[a]	0.450
E	—[a]	—[a]	—[a]	*0.004*	—[a]	0.576	—[a]	*0.012*

	Type G				Type H			
T^*	0.67		2.00		0.67		2.00	
η	0.15	0.45	0.15	0.45	0.15	0.45	0.15	0.45
R	—[a]	0.514	*0.002*	0.150	*7.449*	0.929	0.037	0.157
H	—[a]	*0.055*	0.061	0.493	11.351	*0.204*	0.047	0.256
P	—[a]	2.821	0.068	0.818	49.218	2.310	0.025	0.655
F	—[a]	—[b]	0.050	0.338	—[b]	—[b]	0.073	0.230
E	—[a]	0.457	0.163	*0.011*	9.280	0.217	*0.011*	*0.033*

[a] Simulated system is not a single-phase, uniform fluid at equilibrium.
[b] Theory predicts an unphysical RDF, *i.e.* $g(r) < 0$ for some r.